Scientific Journal for Damietta Faculty of Science **12**(1) 2022, 102-116
DOI: 10.21608/SJDFS.2018.194790
ISSN Print 2314-8594
ISSN Online 2314-8616

https://sjdfs.journals.ekb.eg/

Geology, Petrography and Radioctivity as will as Environmental Impact at Wadi Kab Ar Rakab Al Shamali Rocks, Eastern Desert, Egypt

Mona A.El Hariery[1], Adel El Afandy[2] and Hoda R. Saad[*1]

[1]Geology department, Faculty of Science, Damietta University, New Damietta, Egypt.
[2]Nuclear Materials Authority, Cairo, Egypt.

Received: 10 September 2022 /Accepted: 10 November 2022

[*] Corresponding author's E-mail: hodaragab@hotmail.com

Abstract

This work discusses the geologic setting of Wadi Kab Ar Rakab Al Shamali area in the South Eastern Desert of Egypt, and the distribution of the natural radionuclides and assess the radiological hazard resulting from different rock types in the area. The background radiation levels, human exposure, dose rates, and potential radiation effects on the environment are all studied. The field geological investigation of the different rock units, with orientations to their mode of occurrence, common relationships, petrographic study and regional structure indicated that the investigated area is covered by Late Proterozoic igneous and metamorphic rocks. These basement rocks are included metavolcanics, metagabbros, granodiorites, younger gabbros, monzogranites, syenogranites, alkaline granites and alkaline syenites. The studied rock types have low uranium and thorium contents. The yearly effective dose, external absorbed dose rate in both indoor and outdoor environments, internal absorbed dose rate in both indoor and outdoor environments, and radium equivalent activity are all estimated. The investigation indicates that all the environmental impacts dose rates values in the studied rocks are lower than the public permissible values in these rocks and they are within the safety range for the public and workers. So, these rocks are safe for the building materials and can be used as ornamental stones.

Keywords: Kab Ar Rakab Al Shamali, Radioactivity, Radiological hazards.

Introduction

The Eastern Desert and Sinai are portion of Egypt's basement complex, which also includes Neoproterozoic juvenile crust formed in the Arabian-Nubian Shield (ANS) (Stern, 2002). The (ANS) is a broad region approximately 3 million km^2 in size, of Neoproterozoic crust that spans most of NE Africa and the western portion of the Arabian Peninsula. Its northwesterly portion is made up of the Egyptian basement rocks of the Eastern Desert (ED) and Sinai. The Neoproterozoic juvenile continental crust is thought to be best preserved and exposed in the ANS (Be'eri-Shlevin et al., 2009, 2012; Gradstein et al., 2004; Stern, 2002; Hargrove et al., 2006; Fritz et al., 2013). This crust includes dismembered ophiolites,

volcano-sedimentary successions, and calc-alkaline I-type intrusive complexes. Granitoids constitute vital rock group that covers huge areas of the ANS. In Egypt, granitoids cover about 35,00 Km^2 forming about 35% of the basement rocks. The peraluminous two-mica granites are well-considered to be among the world's most ideal host rocks for U-mineralization (Friedrich et al., 1989; Poty et al., 1986; Cuney et al., 1984). Rb, Nb, Sn, Th, and U are among the odd characteristics of the incompatible elements present in granite (Rameshbabu,1999; Pal et al., 2007). Primordial radionuclides predominantly associated with natural radioactivity include those from the ^{238}U, ^{232}Th, and ^{40}K families. The type of rocks has an impact on the background radiation on Earth. Phosphate, calcrete, and granitic rocks have higher quantities of uranium, thorium, and potassium (Nada, 2003; Nagdya, 2003; Abbady et al., 2005; Harb, et al., 2008; El Aassy, et al.,2012; Hamidalddin, 2012, Walley El-Dine, et al., 2012, Sroor, et al., 2012, Abdel Halim, 2016, Moghazy, 2016 and El Afandy et al., 2018). The members of the individual decay series will have the same activity (Bq/kg) as soon as a geological formation containing ^{238}U and ^{232}Th has not been disturbed (closed system) for more than a million years; this state is referred to as secular equilibrium. However, if the geological formation is not locked to radionuclide migration, ^{226}Ra can move and deposited outside the formation, secular equilibrium will not exist, and development of ^{226}Ra by radioactive decay of its ancestors will not take place. As a result, ^{226}Ra is said to be unconfirmed. Owing to the natural radionuclides' geological mobility, if radiation exposure and dosage rates are higher than allowed, it may have an adverse effect on the environment and human health. Therefore, determining radiation doses from natural sources is essential when they are the primary source of the population's external exposure (UNSCEAR, 2000). This work discusses the geologic setting of Kab Ar Rakab Al Shamali area, and the distribution of the natural radionuclides and assess the radiological hazard resulting from the different rock types in the studied area using NaI (Tl)-ray spectrometers. The background radiation levels in the environment, human exposure, dose rates, and potential radiation effects on the environment were all studied.

Geological setting

The Um Shadad area is mostly covered by Late Proterozoic igneous and metamorphic rocks. These basement rocks exposed in the study area are mainly arranged starting from the oldest as metavolcanics, metagabbros, granodiorites, younger gabbros, monzogrznites, syenogranites, alkaline granites and alkaline syenites. A geological map at scale 1:50000 is prepared for the study area **(Fig. 1).** The field geologic features and relationships of the different rock types with each other and their lithological varieties as well as their petrographic description are discussed in detail as follow:

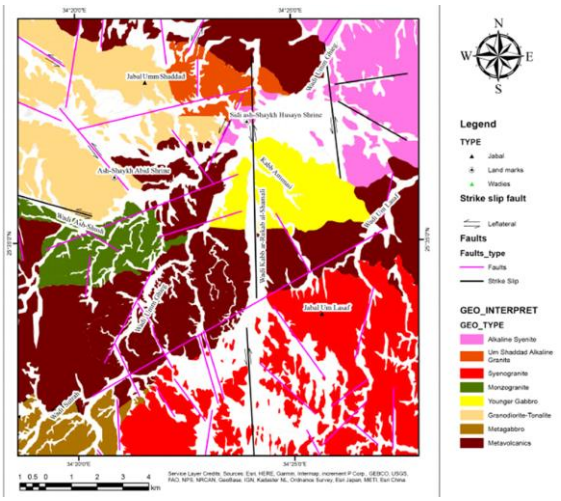

Figure 1. Geological map of the study area (modified after Conoco coral, 1987).

The metavolcanics are exposed along the central and northeastern parts of the studied area (Fig. 1). They are dominantly fine-to medium-grained, massive to moderately foliated, and low to moderate relief. These rocks are grayish green to green in colour with brown alteration surfaces in the field. They cut by W. Kab Al Rakab Al Shamali, Wadi Umm Ghieg and bounded by Wadi Sutrah in the southwestern part of the mapped area. They are intruded from the north by younger gabbros, monzogranites and alkaline syenite and from the south by metagabbros and syenogranites. They cut by N-S, NE-SW, NNE-SSW and NNW-SSE faults. The contacts between these rocks and the surrounded rocks are structural and intrusive. The metavolcanic rocks are represented mainly by metabasalts, metabasalitic-andesites and metaandesites.

The metagabbros are encountered in the southwestern corner of the studied area and extended out of the border of the of the area

constituting a wide belt and cut by Wadi Ash Shush, (Fig. 1). These metagabbros include layered in addition to massive varieties. They are greyish green in colour with brownish or yellowish- brown weathering. Textural and compositional structures of these metagabbros vary from place to place. The layered gabbros are generally banded and showing rhythmic layering. This layering is owing to alternative arrangement of leucocratic and melanocratic bands. These layers have thickness ranging from 1 cm to 3 cm but in other places exhibit much thicker layers ranging in thickness from 1 m to 5 m.

Tonalite-granodiorite assemblages in the study area are characterized by quartz-diorites, tonalites and granodiorites, respectively. These rocks are located in the north western corner of the studied area, (Fig.1). These rocks are denoted by large masses with different sizes. They crop out north Wadi Ash Shushi in the western part of the studied area, (Fig. 1). They intruded metavolcanics and invaded by monzogranites and Um Shadad alkaline granites. These rocks are massive forming low relief hillocks, due to rapid weathering, with smooth slopes and rounded tops, as well as characteristic abundant fracturing. Theses rocks are cut by N-S, NE-SW, NNE-SSW, NW-SE and NNW-SSE faults. The contacts between these rocks and the surrounded metavolcanics, monzogranites and Um Shadad alkaline granites are structural and intrusive contacts.

Younger Gabbros harvest along Wadi Kab El Rakab and create a dark green, medium-relief mass that encroaches on the neighboring metavolcanics from the east, south, and west. They are intruded from the north east by the alkaline syenite. This gabbro intrusion is dissecting by major shear zone trending N-S. Xenoliths of different sizes and shapes from metavolcanics are recorded within the gabbroic intrusions and gabbroic off-shoots are also encountered intruded into the metavolcanics.

Monzogranites crop out in the west central part of the studied area as an elliptical shaped mass (oval-shaped mass) which is striking in NNE-SSW direction. These granites are epizonal and unfoliated mass, which is traversed by faults trending NNW-SSE, NE-SW and NW-SE at the northern part and trending E-W in the southern part. Most of the NNW-SSE and NW-SE faults are of strike-slip type with left-lateral movement. Moreover, these granites have sharp contacts with the tonlalite-granodiorites at their northern contact and with metavolcanics in the southern, eastern and western contacts. The monzogranites show offshoots and apophyses into the surrounding rocks.

Syenogranites rocks in the study area are occur at Gabal Um Lasaf the northern part of Gabal Kadabora. They form an oval shaped ENE trending mass (Fig. 1). These granites crop out at the south eastern part of the mapped area. These granites are traversed by faults trending NNW-SSE, NNE-SSW, NE-SW, N-S and NW-SE direction. They range in colour from pinkish white to pink granites, and grain size from medium to coarse grained. The contacts between the syenogranites and metavolcanics and metagabbros are structural contacts. The metavolcanic rocks receive apophyses from the granitic intrusions. These granites are associated with numerous pegmatite bodies and traversed by swarms of dykes. Xenoliths of older rocks are occasionally observed.

Umm Shaddad Alkaline Granites crop out at the northern parts of the mapped area at Jabal Umm Shaddad, (Fig.1). They form conspicuous mountain ridges. They show sharp intrusive contacts with the surrounding metavolcanics, tonalite-granodiorite and alkaline Syenite rocks. The alkali-feldspar granites are affected by a sinistral strike-slip faults with a N-S, direction resulting in splitting the mass of Jabal Jabal Umm Shaddad into two separate parts, having a general elongation in the E-W direction as well as ENE-WSW, NNE-SSW, and NNW-SSE directions. They are medium to coarse-grained, exfoliated, highly weathered with pinkish red color due to staining with iron oxides. These granites have pink to greyish pink colour. They are of high relief and undeformed. They are hypersolvus composed of K-feldspars (perthites, orthoclase perthites, and antiperthites), quartz and mica.

Alkaline Syenite rocks occupied the north eastern corner of the mapped area. They are usually dark brown to greyish brown in colour and forming low hilly terrain. They range in composition from alkaline syenite to quartz alkaline syenite. They are medium to coarse grains and sometimes porphyritic and form highly weathered terrains. They are intruded the metavolcanics and the younger gabbros and encloses xenoliths of different sizes and shapes from them. They are cut by Wadi Um Gheig from the north and Wadi Um Lasaf from the south. They are cut by NNW-SSE, NW-SE, and

ENE-WSW faults.

Petrography

The metavolcanics, the metabasalts are composed chiefly of plagioclase, actinolite, augite, epidote and iron oxides. The plagioclases encountered form orientation or flow texture and are moderately to intensely altered and twinned according to the albite and carlsbad laws. Actinolite occurs as subhedral fibrous with preserved relics of augite. Amygdales of different sizes of filled with quartz are present. Actinolite is partially altered into chlorite, iron oxides and epidote. Opaque minerals occur as disseminated in the groundmass.

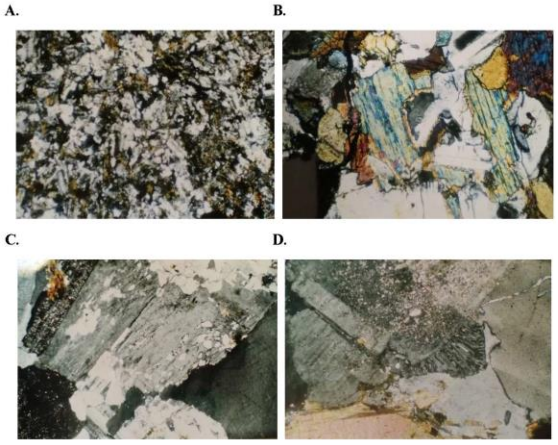

Figure 2. A. Microphotograph in metabasaltic andesite composed of plagioclase laths and augite, x20. **B.** Microphotograph showing subophitic texture and the essential composition of metagabbros, x20. **C.** Microphotograph in tonalite showing poikilitic texture between weak pleochroism plagioclase and quartz, also showing altered plagioclase, x20. **D.** Microphotograph in granodiorite showing myrmicitic texture and sericitized feldspars, x20.

Metabasaltic andesites are composed frequently of plagioclases, actinolite, augite and hornblende. Iron oxides are accessory minerals. The plagioclases sometimes occur as xenocrysts and partially cracked. They are generally present as twinned laths, and sometimes the lamellar twinning is hardly seen due to the alteration of the rock. Actinolite is characterised mainly by allotriomorphic yellowish crystals, transformed to chlorite. It exists in the interstitial spaces between the plagioclase crystals forming intergranular texture. Augite forms irregular relics within actinolite. Hornblende form subhedral crystals with greenish colour, (Fig. 2A). According to the mineralogical assemblage (chlorite + actinolite + epidote + quartz) of these rocks, it is suggested that they were affected by low grade metamorphism (Winkler, 1979).

Metaandesites are composed of plagioclase, hornblende, relics of pyroxenes, occasionally quartz, apatite, chlorite, epidote, actinolite and opaques. Plagioclases occur as tabular xenocrysts of prismatic habit and as small laths forming the major portion of the groundmass. Sometimes, plagioclase xenocrysts are strained, cracked, and fractured. Augite is represented mainly by anhedral yellowish crystals, altered to fibrous amphibole. They are present in the interstitial spaces between the feldspar crystals forming the intergranular texture. Hornblende occurs as prismatic crystals. It shows corroded margins owing to the degrees of replacement by chlorite and actinolite. Quartz forms allotriomorphic crystals occurring as interstitial grains (less common). Pyroxenes are granular randomly oriented in the groundmass. Opaques are found as irregular crystals or fine dissemination, and apatite forms short laths or small needles.

The metagabbros, consist basically of plagioclases, hornblende, and augite with pseudomorphs of chlorite. Accessories include iron oxides, epidote, and apatite. Plagioclases occur as megacrysts and smaller crystals. The plagioclase from euhedral to subhedral crystals. They are existing in the interstitial spaces between augite and hornblende and sometimes showing cumulus with mafic minerals (augite, hornblende, and epidote). Augite is present as relics and is partly or completely altered to hornblende (uralitization), and chlorite. Hornblende is existing in significant amounts and occurs as coarse and fine crystals. It forms idiomorphic to subidiomorphic prismatic green crystals with strong pleochroism. Opaques and epidote are found coupled with hornblende and augite. Apatite is rare and usually occurs as prismatic needles in association with hornblende and plagioclase. The rock is interpreted as uralitized gabbro, (Fig. 2B).

Tonalite-granodiorite, are composed mostly of plagioclases, quartz, and hornblende. K-feldspar forms minor constituent not exceeding 5% of the total amount of the feldspars. Minor amounts of biotite are found in some samples. Zircon is present as accessory minerals. Plagioclases occur as subhedral to anhedral

sercitized crystals. Zoning is occasionally recorded in the coarse plagioclase crystals but is generally weak, (Fig. 2C). Some plagioclase crystals poiklitically incorporated within deformed quartz crystals, others corroded marginally with quartz. Quartz occurs as medium to coarse anhedral crystals or crystal aggregates. Greatest of the quartz crystals exhibit strong undulatory and shadowy extinction due to deformation. The mafic minerals are represented chiefly by hornblende, which form subhedral crystals, partially altered to chlorite and epidote and mottled with iron oxides. Some hornblende crystals are bleached and altered to opaque minerals. In some cases, they seem to be micro folded and lineated in agreement with the surrounding minerals. Hornblende is pleochroic from yellowish brown to dark brown. Biotite is rarely observed in these rocks. Few deformed orthoclase crystals are observed. Zircon occurs as individual euhedral crystals up to 0.02 mm long, or as tiny prisms enclosed in feldspars and quartz.

The quartz diorites are composed of plagioclase, hornblende, biotite, muscovite and quartz together with accessory opaque minerals, sphene, apatite and zircon. Plagioclases occur as large subhedral prismatic crystals up to 3mm in length and 1mm in width. They are saussuritized to numerous degrees in the cores of normally zoned crystals and the rims still fresh. It is usually twinned according to albite, microcline and combined albite-carlsbad laws. Hornblende occurs as long subhedral prismatic crystal ranging from 0.5 to 1.5 mm in length and from 0.3 to 0.6 mm in width. It has a deep green to yellowish green color pleochroism. It may display simple twinning and includes several short prisms of zircon, quartz blebs and plagioclase clusters. Biotite present as subhedral to anhedral flakes, strongly pleochroic from yellowish brown to dark brown. It is slightly to strongly chloritized and charged with opaques along cleavage planes. Opaque minerals occur as irregular grains enclosed in hornblende and chlorite and generally rimmed by sphene.

The granodiorities are mainly composed of plagioclase and quartz together with lesser microcline, biotite and hornblende. Accessories are opaques, zircon, apatite and sphene. Plagioclases occur as subhedral to euhedral prismatic crystals ranging from 0.7 to 4 mm length and from 0.3 to 2.5 mm in width. It is usually altered to serecite especially in the cores, may also occurred in some plagioclase crystals, (Fig.2d). Biotite occurs as prismatic crystals and flakes. It is pleochroic from dark brown to yellowish brown. The biotite sometimes altered to chlorite and sometimes contains apatite and sphene inclusions. Opaques, apatite, zircon and sphene crystals stand as accessory minerals. Chlorite occurs as subordinate mineral after biotite, it is strongly pleochroic from pale yellowish green to grass green.

Younger Gabbros, these rocks are medium to coarse grained, dark green in colour, and composed of plagioclases and clinopyroxene with subordinate amounts of actinolite and iron oxides. It is characterized by ophitic textures. Plagioclases occur as euhedral to subhedral tabular crystals ranging from 0.7 x 1.9 mm to 1.2 x 2.6 mm, displaying albite and pericline twining and variable degrees of alteration to serecite. Clinopyroxenes are represented by subhedral diopside and short prismatic augite, weakly pleochroic from pale green to colourless. Clinopyroxenes enclose ophitically plagioclase crystals. They are commonly altered to actinolite and chlorite. Actinolite occurs as anhedral crystals or crystal aggregates with pale green colour and faint pleochroism. Iron oxides occur as small euhedral crystals bounded in the clinopyroxenes.

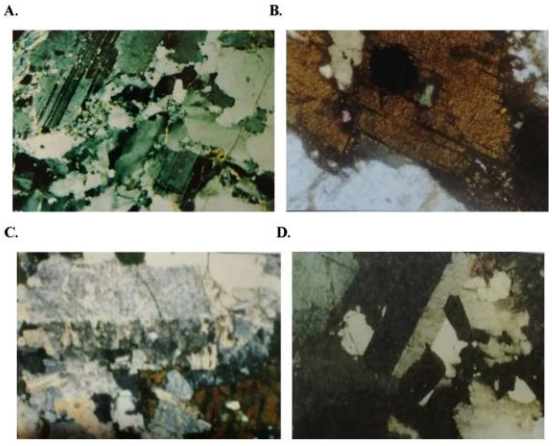

Figure 3. A. Microphotograph in monzogranite showing the high deformation of plagioclase, x20. **B.** Microphotograph in syanogranite showing subhedral plate of biotite and enclosing zircon and opaque minerals, x20. **C.** Microphotograph in alkali granite showing perthite, plagioclase, quartz and rebeikite, x20. **D.** Microphotograph in alkali syenite showing perthite, x20.

Monzogranites, these rocks are basically composed of potash feldspars, quartz, plagioclases and biotite with subordinate

hornblende. Zircon, allanite apatite and iron oxides are the chief accessories whereas chlorite, sericite, muscovite and kaolinite are secondary alteration minerals, (Fig. 3a). Potash feldspars are represented mainly by microcline and microcline perthites of string and patch types. Sometimes they are found to include plagioclase and quartz crystals. Quartz arises as coarse and fine anhedral crystals. The coarse crystals are anhedral to subhedral showing undulous extinction due to deformation. The fine crystals are mostly included within K-feldspars, plagioclases, and mafic constituents. Plagioclase forms anhedral to subhedral tabular crystals. Plagioclase crystals are fresh and exhibit twinning according to albite or microcline laws. In other cases, plagioclase is zoned and partly altered specially at the core. Minute inclusions of biotite, apatite and iron oxides are enclosed within some of the plagioclase crystals. Biotite forms elongated flakes or aggregates with other mafic constituents. Biotite is yellowish brown in colour and pleochroic from yellowish brown to dark brown. Sometimes biotite contains tiny crystals of zircon and apatite. Hornblende is observed in some samples of monzogranite. It is strongly pleochroic with pale green, yellowish green and dark green colour. Sometimes it is crowded with inclusions of opaques along cleavage traces. Zircon forms prismatic crystals mainly included within biotite flakes. Allanite occurs as elongated crystals (six-sided). It is strongly pleochroic from pale brown to dark brown and zoned. Chlorite occurs as secondary alteration mineral after biotite and hornblende. Apatite forms short prismatic crystals and is commonly included within biotite, plagioclase and quartz.

Syenogranites, these granites are holocrystalline exhibiting hypidiomorphic granular texture. They are generally medium to coarse-grained and non-porphyritic. The essential constituents are potash feldspars, quartz, plagioclases and minor biotite. The accessory minerals are zircon, apatite, allanite and iron oxides. The potash feldspars are characterized by orthoclase and microcline perthites stained by iron oxides along the cleavage planes which is probably responsible for the conspicuous reddish colour imparted to these granites. The crystals are corroded by quartz and sometimes altered to sericite. Quartz is present as anhedral to subhedral crystals, sometimes reaching up to 5mm across. Quartz is sometimes deformed and shows strong wavy extinction. Plagioclase form subhedral to anhedral tabular crystals and exhibit twin lamella of albite or percline law. Zoning is occasionally observed in the coarse plagioclase crystals. Biotite forms subhedral flakes, sometimes with torn ends enclosing zircon and iron oxides, (Fig. 3B). Biotite is sometimes altered to chlorite. Iron oxides occur as anhedral skeletal grains in association with biotite. Allanite form zoned prismatic crystals. Zircon is commonly found as inclusions in biotite.

Umm Shaddad Alkaline Granites, is characterized by equigranular and holocrystalline texture and the by the presence of alkali amphibole riebeckite as mafic minerals. Abundant microcline perthite is the main constituent of these rocks. These granites are composed of Plagioclase, microcline perthites and quartz large crystals that are associated with medium-grained microcline and quartz, (Fig. 3c). The accessories are zircon, titanite and opaque. K-feldspars occur as large microcline perthite crystals. The perthite intergrowths show different shapes like patches; flame, string and spindle shaped perthites. K-feldspar large crystals are interlocked with quartz and riebeckite crystals and contain inclusions of zircon. Quartz presents as anhedral crystals. It has oval and ribbon shapes and usually includes K-feldspar and mafic inclusions. Quartz exhibits strong wavy extinction and characteristic light gray colour. Plagioclases are present in notable amount and form large euhedral prisms with clear albite twining. The alkali amphibole mineral riebeckite is present in a notable amount in these granites indicating their alkaline affinities. Rebikite has light green to dark green color. It shows the characteristic amphibole cleavage and pleochroism.

Alkaline Syenite, these rocks are composed of alkali feldspar perthites and antiperthite, plagioclases, and quartz. Mafic minerals are represented by aegirine, aegirine augite and arfvedsonite, while iron oxides, sphene and zircon are accessory minerals. Orthoclase perthite occurs as tabular crystals and constitute most of the rock composition (Fig. 3D). The contacts between the perthite crystals are irregular with intergrowths of secondary albite which may show reaction zones on these boundaries and sometimes exhibits fine lamellar twinning. Secondary quartz protrudes into perthite crystals and may be observed in

association with secondary albite. Primary, still-young plagioclase crystals have some antiperthitization, mainly on the crystal edges. Secondary albite is present and protrudes all other minerals. Minor amounts of interstitial clear quarts are present in the syenites. Quarts is essentially of secondary origin as it protrudes into all other minerals. Mafic minerals are represented mainly by aegirine, aegirine augite and arfvedsonite. Aegirine and aegirine augite occur as elongated prismatic crystals. They are strongly pleochroic with the most communal pleochroic. Orthoclase crystals are sometimes ophitically or subophitically included in aegirine. Arfvedsonite forms subhedral prismatic crystals. It is strongly pleochroic. It is generally corroded with perthite, secondary albite and quartz.

Analytical Techniques

Sixty-three representative samples from the different rock types in the studied area were being filled and tightly sealed, cylindrical cans made of plastic with a 212 cm2 volume, 9.5 cm diameter, and 3 cm height were left for more than 30 days to gather free radon and reach radioactive equilibrium before being counted with a -ray spectrometer and then subjected to laboratory tests at the Egyptian Nuclear Material Authority to determine eU, eTh, Ra, and K%. And then measured in the radiometric lab in Nuclear Materials Authority for their eU, eTh, and K% contents using a high efficiency multichannel analyzer of-ray spectrometer NaI (Tl). These radionuclides' radiometric measurements were authorized over four energy ranges. Thorium was measured indirectly using the gamma-ray photons released by their daughters, Th-234 (81-108 keV) for U-238 and Pb-212 (221-273 keV) for Th-232. Radium was measured using the gamma-ray photon released by Pb-214 (327-390 keV), uranium was measured using the gamma-ray photon released by K-40 (1319-1471 keV). As a result, they are written as equal amounts of uranium (eU), thorium (eTh), and radium (eRa). The specified energy lines of the spectra produced with laboratory uranium, thorium, radium, and potassium orientation reference samples provided by the IAEA were used to estimate the chosen energy regions for U, Th, Ra, and K. (Matolin, 1991). The samples were prepared for measurement according to procedures described by (Matolin, 1991; Al-Jundi, 2002, Hamby and Tynybekov, 2000). Utilizing the conversion factors provided by the Polish Central Laboratory for Radiological Protection, values of eU, eTh, and eRa, in ppm, as well as K, in%, were converted to activity concentration, Bq/kg (Malczewski et al., 2004). These data used to construct some radiological parameters to evaluate the radionuclides' effects on the environment, as will be shown later.

Results and discussions

Radioactivity analysis

The spreading of detected radionuclides, ^{238}U (ppm), ^{232}Th (ppm) and ^{40}K (%) in the studied rock samples are shown in Table 1. eU, eTh, and K radioelement contents varied from 0.5% to 1.8% with an average of 1.1%, from 2 to 6.3 ppm with average of 3.4 ppm, and from 0.5% to 1.8% with an average of 1.4% for the metavolcanics respectively. Radioelement abundance in metagabbro ranged from 0.5 to 2 ppm with average of 1.3 ppm for eU, from 2.5 to 6 ppm with an average value of 3.85 ppm for eTh, and from 0.35% to 0.76% with an average value of 0.51% for K. Radioelement concentrations in granodiorites varied from 1 to 3.5 ppm, with average value of 2.2 ppm for eU, from 2.8 to 5.5 ppm, with average of 4.32 ppm for eTh, and from 2.3% to 3.5%, with average of 2.78% for K. The radioelement content of the younger gabbros ranges from 0.7 to 2.3 ppm with average of 1.38 ppm, from 1.3 to 2.5 ppm with average of 2.4 ppm, and from 0.6% to 1.2% with average of 0.88% for eU, eTh, and K, respectively. eU concentration in monzogranites ranged from 1.1 to 6.3 ppm with average of 3.3 ppm, eTh content ranges from 5.8 to 9.3 ppm with an average of 7.62 ppm, and K content range from 2.6% to 4% with average of 3.38%. Radioelement concentrations in Syanogranites range from 3 to 11 ppm, with average of 6 ppm for eU, from 9 to 21 ppm, with an average of 13.75 ppm for eTh, and from 3.5% to 4.7%, with average of 4.15% for K. Additionally, the radioelement concentration of alkaline granites ranges from 2 to 9 ppm, with average of 4.3 ppm for eU, from 7 to 15 ppm, with average of 11.2 ppm for eTh, and from 3.1% to 4.2%, with average of 3.75% for K. and radioelement concentrations in alkaline syenites are 1 to 4 ppm with average of 2.7 ppm for eU,

2.9 to 10 ppm with average of 6.58 ppm for eTh, and 3% to 3.6% with average of 3.28% for K.

Table 1. eU, eTh, and K contents of the studied rocks.

Rock type	U	Th	K%
Alkaline Syenites	4	9	3.6
	3	10	3.5
	1	5	3.0
	3	2.9	3.1
	2.5	6	3.2
Alkaline Granites	3	9	3.4
	2	5	3.6
	4	13	4.2
	4	14	4.1
	3	11	3.5
	5	13	3.7
	4	7	3.6
	9	15	4.2
	5	13	3.7
	4	12	3.5
Syenogranites	4	11	4.2
	3	9	3.8
	6	10	4.2
	5	12	4.3
	11	21	4.6
	6	18	4.7
	5	14	3.7
	8	15	3.5
Monzogranites	2.8	8.4	3.2
	3.7	8.7	4.0
	1.6	5.9	2.8
	1.1	7.6	2.6
	6.7	5.8	3.8
	3.7	9.3	3.9
Younger Gabbros	0.7	1.3	0.6
	1.3	2.9	0.8
	1.2	2.9	0.7
	2.3	2.6	1.2
	1.4	2.3	1.1
	1.3	3	2.5
Granodiorites-Tonalites	2.7	5.5	3.2
	1	4	2.4
	1.7	4.5	2.6
	1	2.8	2.8
	2	3.8	3.0
	3.5	4.8	3.5
	2.8	4	3.0
	3	4.7	2.8
	2.5	5.4	2.3
	2.6	5	2.4
Metagabbros	2	5	0.70
	1.5	3	0.40
	0.5	3	0.45
	1	2.5	0.40
	2	3	0.35
	0.5	3.5	0.40
	1.5	5	0.60
	1.4	3.5	0.65
	1.6	6	0.76
	1	4	0.40
	2	6.3	1.8
	1	2.5	1.2
	2	3	0.9
Metavolcanics	1.5	4	1.4
	1	3	0.6
	1.6	3	1.3
	1	2	0.5

Evaluation of radiological hazard effect

Using the conversion factors provided by the Polish Central Laboratory for Radiological Protection and the International Atomic Energy Agency (IAEA, 1989), K, in% and the values of eU and eTh in ppm were converted to activity concentration, Bq/kg (El Galy et al., 2008; Malczewski et al., 2004). A sample comprising 1 ppm, by weight, of U, 1 ppm, by weight, of Ra, 1 ppm, by weight, of Th, and 1 ppm, by weight, of 40K has a specific parent activity of 12.35 Bq/kg, 11.1 Bq/kg, and 313 Bq/kg, respectively. Therefore, by calculating the following parameters, it may be simple to estimate the consequences of this radiation.

Radium equivalent activity, Ra_{eq}

The action of radioactive decay built on the idea that 370 Bq/ kg of ^{238}U, 259 Bq/ kg of ^{232}Th, and 4810 Bq/kg of ^{40}K produce the same rate of gamma ray dosage, Ra_{eq} is a weighted sum of the activity of the radionuclides ^{238}U, ^{232}Th, and ^{40}K. (Beretka and Mathew, 1985)

$$Ra_{eq} = A_U + 1.43\ A_{Th} + 0.077\ A_K \quad (1)$$

wherever A_U, A_{Th} and A_K are the specific activities of ^{238}U, ^{232}Th and ^{40}K in Bq/ kg. Ra_{eq} assessed for the collected rock samples and are given in Table 2. The values obtained fall short of the permitted global threshold (370 Bq/kg).

Gamma activity index, $I_{\tilde{a}}$

Construction material constraints for gamma radiation are based on a dose range of 0.3 to 1 mSv/y (Tzortzis et al., 2003). The $I_{\tilde{a}}$ was derived from equation 2 to determine whether a construction material satisfies these restrictions of dosage criteria (Tzortzis et al., 2003):

$$I_\gamma = \frac{A_U}{300} + \frac{A_{Th}}{200} + \frac{A_K}{3000} \quad (2)$$

The amounts of ^{238}U, ^{232}Th, and ^{40}K, respectively, are expressed as A_U, A_{Th}, and A_K in Bq/kg. The formula above is built on the observation that radionuclides donate to external radiation in proportion to their individual exposure rate constants, i.e., ^{40}K: ^{238}U: ^{232}Th = 1:10:15. This method calculates an index of gamma irradiation using the total of three distinct activity quotients, with the denominators selected to reflect the distinct exposure rate and provide a sum of one. According to Tzortzis et al. (2003) and Anjos, (1999), $I_{\tilde{a}} \leq 6$ corresponds to a dosage criterion

of 1 mSv/y for the activity concentration index, while $I_{\tilde{a}} \leq 2$ corresponds to a dosage criterion of 0.3 mSv/y (Akram et. al., 2005). As a result, the activity concentration index should only be used as a screening tool to find materials that could be problematic when used as building or covering materials. Materials with $I_{\tilde{a}} \geq 6$ should be avoided in accordance with this dosage criterion since these values correspond to dose rates more than 1 mSv/y (EC, 1999), the maximum recommended dose rate in air for the general population (UNSCEAR, 1993, 2000). For each type of rock, the computed value of $I_{\tilde{a}}$ and its average values are listed in (Table 2). The gamma activity index averages for the eight different types of rocks are below the permissible level (2). Additionally, it can be shown from the data that the analyzed rock samples had $I_{\tilde{a}} > 1$ that correlate to dosage rates less than 1 mSv/y, which is the smallest value of airborne dosage rate that is thought to be safe for population (UNSCEAR, 1993, 2000).

Alpha Activity index, $I_{\acute{a}}$

Radon descendants release radioactive alpha particles as they decompose, which adhere to aerosols, dust, and other airborne particles. The alpha particles from (Ra) progeny that are left on the cells lining our airways during inhalation could damage DNA and lead to lung cancer. To measure the degree of exposure owing to (Ra) inhalation initiating from building materials, several alpha indices have been developed (European Commission (EC), 1999). (Krieger, 1981). To assess the excess alpha radiation caused by radon inhalation from building materials, the alpha index ($I_{\acute{a}}$), which is defined in (eq.3) of Zubair et al. (2013); Righi and Bruzzi (2006); Bavarnegin et al. (2013);

$$I_{\alpha} = \frac{A_U}{200} \leq 1 \qquad (3)$$

The activity level of ^{238}U is A_U. According to ICRP, 1994, the proposed exception and upper border of ^{238}U activity conc. in construction materials are 100 and 200 Bq/kg, respectively. The highest ^{238}U concentration that is advised is 200 Bq/kg, which results in $I_{\acute{a}} = 1$. It is conceivable for radon exhalation from any construction material whose ^{226}Ra activity concentration surpasses this upper limit (200 Bq/kg) to raise indoor radon concentrations above this limit.

Values of $I_{\acute{a}}$ for each type of rocks and its average values are listed in (Table 2). We can see that the $I_{\acute{a}}$ values are below the permitted level. Therefore, it can be claimed that the risk of radon inhalation from structures made of these materials is so low that their usage in building construction should be limited.

Hazard indices (H_{ex} and H_{in})

External hazard index, H_{ex}

The H_{ex} is used to quantify the external risk brought on by gamma radiation emissions. Equation 4 (after Fares, et al., 2012; Orgun et al., 2007; Beretka and Mathew, 1985) was used to calculate it as follows:

$$Hex = \frac{AU}{370} + \frac{ATh}{259} + \frac{AK}{4810} \leq 1 \qquad (4)$$

A_U, A_{Th}, and A_K are the specific activity of ^{238}U, ^{232}Th, and ^{40}K, in Bq/kg, respectively. By assuming that the external hazard index's maximum permissible value (equal to unity) corresponds to Ra_{eq}'s upper limit (370 Bq/kg), H_{ex} can be calculated using Ra_{eq} equation. To be considered minimal, the radiation risk from construction materials must have a value of this index lower than unity (Hayumbu et al., 1995). The highest value of Ra_{eq} must be less than 370 Bq/kg for H_{ex} to have a maximum value that is less than unity. H_{ex} values for several types of rocks are provided in addition to their average values in (Table 2). The values of the external hazard index are lower than the permitted value, as can be seen from the calculated H_{ex} values. Therefore, where the readings correlate to radium equivalent values below the maximum limit, the radiation risk from these rocks can be insignificant (370 Bq kg^{-1}).

Internal hazard index, H_{in}

The internal exposure to ^{222}Ra and its radioactive offspring is managed by the internal hazard index (H_{in}). In eq.5 (Fares, et al., 2012; Orgun et al., 2007; Beretka and Mathew, 1985), it is stated as follows:

$$Hin = \frac{AU}{185} + \frac{ATh}{259}\frac{AK}{4810} \leq 1 \qquad (5)$$

The conc. of ^{238}U, ^{232}Th, and ^{40}K in Bq/kg are denoted as A_U, A_{Th}, and A_K, respectively. H_{in} will be less than 1 if the maximum uranium content in the study samples is half of the typical permitted limit (Beretka and Mathew, 1985). H_{in} should be less than unity for the safe usage of a material in the construction of a house (Beretka and Mathew, 1985). For each of the rock types and samples analyzed, values of

H_{in} are determined, along with their average values, and listed in (Table 2). The H_{in} results show that the average values are lower than the permissible value, which means that there is no radiation risk to the respiratory organs from these samples, allowing them to be used as a safety material in residential construction.

Table 2. Radium equivalent activity (Ra_{eq}), Gamma activity level (I), activity index (Iá), hazard indices (H_{ex} and H_{in}) absorbed dose rate ($D_{out\ \&in}$)), and Annual effective dose (AEDE $_{out\ \&in}$) of the studied rocks.

Rock Types	Ra_{eq}	I	Iá	H_{ex}	H_{in}	D_{out}	D_{in}	AEDE $_{out}$	AEDE $_{in}$
Alkaline Syenites	188.42	0.72	0.25	0.50	0.64	9.213	12.897	0.11	0.45
	179.46	0.69	0.19	0.48	0.58	8.753	12.255	0.11	0.43
	113.68	0.46	0.06	0.31	0.34	5.774	8.084	0.07	0.28
	128.60	0.51	0.19	0.35	0.45	6.534	9.148	0.08	0.32
	142.83	0.56	0.15	0.39	0.47	7.122	9.971	0.09	0.35
Average	150.60	0.59	0.17	0.41	0.50	7.479	10.471	0.09	0.37
Alkaline granites	171.25	0.66	0.19	0.46	0.56	8.382	11.735	0.10	0.41
	140.49	0.56	0.12	0.38	0.45	7.142	9.998	0.09	0.35
	226.1	0.87	0.25	0.61	0.74	10.966	15.350	0.13	0.53
	229.50	0.88	0.25	0.62	0.75	11.068	15.496	0.14	0.54
	185.27	0.71	0.19	0.50	0.60	8.990	12.587	0.11	0.44
	226.40	0.86	0.31	0.61	0.78	10.856	15.198	0.13	0.53
	176.80	0.68	0.25	0.48	0.61	8.739	12.234	0.11	0.43
	299.46	1.11	0.56	0.81	1.11	14.247	19.946	0.17	0.70
	226.40	0.86	0.31	0.61	0.78	10.856	15.198	0.13	0.53
	203.42	0.77	0.25	0.55	0.68	9.789	13.704	0.12	0.48
Average	208.51	0.80	0.27	0.56	0.71	10.104	14.145	0.12	0.50
Syenogranites	214.49	0.83	0.25	0.58	0.71	10.492	14.689	0.13	0.51
	180.87	0.70	0.18	0.49	0.59	8.919	12.487	0.11	0.44
	233.38	0.89	0.37	0.63	0.83	11.378	15.929	0.14	0.56
	235.05	0.90	0.31	0.63	0.80	11.425	15.995	0.14	0.56
	368.63	1.36	0.68	0.99	1.36	17.329	24.261	0.21	0.85
	291.88	1.10	0.37	0.79	0.99	13.944	19.522	0.17	0.68
	232.20	0.88	0.31	0.63	0.79	11.093	15.530	0.14	0.54
	270.24	1.00	0.49	0.73	1.00	12.746	17.844	0.16	0.63
Average	253.35	0.96	0.37	0.68	0.88	12.166	17.032	0.15	0.60
Monzogranites	160.47	0.62	0.17	0.43	0.53	7.859	11.003	0.10	0.39
	192.61	0.75	0.23	0.52	0.64	9.510	13.314	0.12	0.47
	121.50	0.48	0.10	0.33	0.38	6.056	8.478	0.07	0.30
	120.37	0.47	0.07	0.32	0.36	5.909	8.273	0.07	0.29
	208.00	0.79	0.41	0.56	0.78	10.239	14.335	0.13	0.50
	193.68	0.75	0.23	0.52	0.65	9.518	13.325	0.12	0.47
Average	166.11	0.64	0.20	0.45	0.56	8.182	11.455	0.10	0.40
Younger Gabbros	30.65	0.12	0.04	0.08	0.11	1.507	2.110	0.02	0.07
	52.17	0.20	0.08	0.14	0.18	2.491	3.488	0.03	0.12
	48.53	0.18	0.07	0.13	0.17	2.301	3.221	0.03	0.12
	72.42	0.27	0.14	0.20	0.28	3.519	4.927	0.04	0.17
	57.15	0.22	0.09	0.15	0.20	2.808	3.931	0.03	0.14
Average	52.19	0.20	0.09	0.14	0.19	2.525	3.535	0.03	0.12
Granodiorites	93.72	0.38	0.08	0.25	0.30	4.798	6.717	0.06	0.24
	142.40	0.56	0.17	0.38	0.47	7.116	9.963	0.09	0.35
	93.42	0.37	0.06	0.25	0.29	4.732	6.625	0.06	0.23
	109.78	0.43	0.10	0.30	0.35	5.512	7.717	0.07	0.27
	96.09	0.39	0.06	0.26	0.29	4.985	6.979	0.06	0.24
	119.07	0.47	0.12	0.32	0.39	6.052	8.472	0.07	0.30
	155.45	0.61	0.22	0.42	0.54	7.802	10.923	0.10	0.38
	130.11	0.51	0.12	0.35	0.44	6.548	9.168	0.08	0.32
	131.82	0.51	0.19	0.36	0.46	6.558	9.181	0.08	0.32
	117.66	0.45	0.15	0.32	0.40	5.772	8.080	0.07	0.28
	118.98	0.46	0.16	0.32	0.41	5..67	8.214	0.07	0.29
Average	118.95	0.47	0.13	0.32	0.39	5.977	8.376	0.07	0.29
Metagabbros	70.60	0.26	0.12	0.19	0.26	3.248	4.547	0.04	0.16
	45.58	0.16	0.09	0.12	0.17	2.090	2.926	0.03	0.10
	34.44	0.13	0.03	0.09	0.11	1.596	2.234	0.02	0.08
	36.50	0.13	0.06	0.10	0.13	1.691	2.367	0.02	0.08
	50.55	0.18	0.12	0.14	0.20	2.304	3.225	0.03	0.11
	36.14	0.13	0.03	0.10	0.11	1.647	2.306	0.02	0.08
	62.01	0.23	0.09	0.17	0.22	2.833	3.966	0.03	0.14
	53.28	0.20	0.09	0.14	0.19	2.488	3.483	0.03	0.12
	72.91	0.27	0.10	0.20	0.25	3.340	4.677	0.04	0.16
	45.21	0.16	0.06	0.12	0.16	2.046	2.865	0.03	0.10
Average	50.72	0.18	0.08	0.14	0.16	2.328	3.2.60	0.03	0.11

Metavolcanics	104.66	0.40	0.12	0.28	0.35	5.033	7.046	0.06	0.25
	55.79	0.22	0.06	0.15	0.18	2.766	3.871	0.03	0.14
	63.81	0.24	0.12	0.17	0.24	3.042	4.259	0.04	0.15
	75.49	0.29	0.09	0.20	0.25	3.670	5.138	0.05	0.18
	44.23	0.16	0.06	0.12	0.15	2.078	2.909	0.03	0.10
	68.51	0.26	0.10	0.19	0.24	3.355	4.697	0.04	0.16
	36.01	0.13	0.06	0.10	0.13	1.707	2.389	0.02	0.08
Average	64.07	0.24	0.09	0.17	0.22	3.093	4.3.30	0.04	0.15
World Value	370	≤2	≤1	≤1	≤1	≤1	59	0.7	0.7

External dose from naturally occurring radionuclides

External absorbed dose rate in outdoor air, D_{out}

The rates of external dosage absorption, the activities of terrestrial radionuclides can be used to compute D_{out} in outdoor air at 1 m above ground level for the inhabitants (Kohshi et al., 2001):

$$D = AE_i \times C_F \quad (6)$$

$$D_{in} = D_{out} \times 1.4 \quad (7)$$

where CF is the dosage conversion factor and A_{Ei} is the activity concentration (Bq/kg) (absorbed dosage rate in air per unit activity per unit mass in units of nGy/h per Bq/kg). Over the past 40 years, a lot of studies have estimated dose conversion factors. The dosage rate conversion factors for ^{238}U, ^{232}Th, and ^{40}K used in this study were those established by Quindos et al. (2004), where C_U= 0.4551, C_{Th}= 0.5835, and C_K= 0.0429. We can see that the values of the external absorbed dose rates are lower than the permitted value since the values of D_{out} for all investigated rock samples and its average values are presented in (Table 2).

External absorbed dose rate in indoor air, D_{in}

Since the research samples are often used in home building, it's important to determine how much of an indoor exposure they provide. According to UNSCEAR (2000), the inside contribution is 1.4 times greater than the outdoor dose, hence the indoor dose rate was also determined.

Values of D_{in} are calculated for all the examined rock samples and the average values for each rock types. We noted that the average dosage rates (D_{out} and D_{in}) for the rock samples are more than the acceptable Egypt levels given in the UNSCEAR (2000) report while being lower than acceptable world values (Table 2).

Annual effective dose, AEDE

With an indoor occupancy of 80% and an outdoor occupancy of 20%, the absorbed rate was converted to the comparable effective dose for humans using a conversion factor of 0.7 Sv/Gy. The annual estimated average effective dose equivalent (AEDE) established by a person was computed using this formula (UNSCEAR, 1993). The annual effective dosage is determined using equations (eqs. 8 and 9):

$$AEDE\ (outdoor) = D_{out}\frac{nGy}{h} \times 8760\ h \times 0.7\frac{Sv}{Gy} \times 0.2 \quad (8)$$

$$AEDE\ (indoor) = \frac{D_{in}\,nGy}{h} \times 8760\ h \times 0.7\frac{Sv}{Gy} \times 0.8 \quad (9)$$

Results shown in table (2) showed that using the aforementioned eqs., the yearly effective dosages for babies and kids may too be calculated while taking into consideration the corresponding UNSCEAR (2000) conversion factors for children and infants of 0.8 and 0.9. The findings from Table 2 suggested that the average yearly effective dose equivalent values for the tested rocks were lower than the global average.

Summary and Conclusions

The studied area is covered by Late Proterozoic igneous and metamorphic rocks, according to the results of the field geological investigation of the various rock types, with references to their mode of occurrence, communal relations, petrographic study, and regional structure. These basement rocks are arranged from oldest to youngest as metavolcanics, metagabbros**,** granodiorites**,** younger gabbros, monzogranites, syenogranites, alkaline granites and alkaline syenites. The studied rocks have low U, Th and K contents. The average contents of uranium are 1.44ppm, 1.3ppm, 2.2ppm, 1.38ppm, 3.3ppm, 6ppm, 4.3ppm and 2.7ppm for metavolcanics, metagabbros**,** granodiorites**,** younger gabbros, monzogranites, syenogranites, alkaline granites and alkaline

syenites. The average values of thorium contents in these rocks are 3.42ppm, 3.85ppm, 4.32ppm, 2.4ppm, 7.62ppm, 13.75ppm, 11.2ppm and 6.58ppm, respectively. The excess values of U and Th contents in syenogranites are due to the high contents of U and Th bearing minerals in these rocks. In the studied rocks, the annual effective dose (AEDE), annual gondal dose equivalent (AGDE), excess lifetime cancer risk (ELCR), Ra_{eq}, I, Iá, Hex, H_{in}, external absorbed dose rates, D_{out} and D_{in}, are all below the public permissible values. So, all the different rocks in the area under consideration are safe for the building materials and ornamental stones.

Declaration of Competing Interest

The authors reaffirm that they are not aware of any personal or financial conflicts that might have appeared to affect the research described in this paper.

References

Abbady, AG E, Uosifand, MAM, and El-Taher A, (2005). Natural radioactivity and dose assessment for phosphate rocks from Wadi El-Mashash and El-Mahamid Mines, Egyptin -Journal of Environmental Radioactivity 84(1):65-78 ·

Abdel Halim ES, (2016). Evaluation of natural radioactivity and excess lifetime cancer risk due to gamma dose rates from Egyptian black sand and its components. Journal of Physical Science and Environmental Studies. 2(2): 30-37.

Ajibode MO, Avwiri GO and Agbalagba EO, (2013). Evaluation of radiation hazard indices in an oil mineral lease (oil block) in Delta State, Nigeria. International Journal of Engineering and Applied Sciences.Vol. 4, No. 2.

Akram M, Qureshi RM, Ahmad N, Solaija TJ (2005). Gamma-emitting radionuclides in the shallow marine sediments off the Sindh coast, Arabian Sea. Radiat. Protect. Dosim. 118(4):440-447.

Al-Jundi J., (2002). Population doses from terrestrial gamma exposure in areas near to old phosphatemine, Russaifa, Jordan. Radiat.*Arabian J. Geosciences*, Meas. 35, 23e28.

Bavarnegin, E. Vahabi, M. Moghaddam, and Fathabadi , N. (2013).Natural radionuclide and radiological assessment of building materials in high background radiation areas of Ramsar, Iran. J Med Phys. 2013 Apr-Jun; 38(2): 93-97.

Be' eri-Shlevin Y, Katzir Y, Whitehouse MJ and Kleinhanns IC, (2009). Contribution of PrePan-African crust to formation of the Arabian Nubian Shield: new secondary ionization mass spectrometry U– Pb and O studies of zircon. Geology37, 899– 902.

Be' eri-Shlevin Y, Samue, MD, Azer MK, Rämö OT, Whitehouse MJ and Moussa HE, (2011). The late Neoproterozoic Ferani and Rutig volcano-sedimentary successions of the northernmost Arabian-Nubian Shield (ANS): New insights from zircon U-Pb geochronology, geochemistry and O-Nd isotope ratios. Precambrian Research 188, 21-44.

Beretka J, and Mathew PJ (1985). Natural radioactivity of Australian building materials, industrial wastes and by-products.Health Phys. 48,87e95.

Conoco Coral, (1987). The Geological map of Egypt (Gabal Hamata). Institute fur Angewandte Geodasie, Berline Techniche Fachhochashule Berline, 1987.

Cuney M; Le fort P, and Wang ZX (1984). Uranium and Thorium Geochemistry and Mineralogy in the Manasluleucogranite (Nepal, Himalaya): Geology of Granites and Their Metallogenetic Relations (Proc. Symposium), Nanjing, 1982, Univ. Sciences Editions, 853-873.

EC (1999). European Commission Report on " Radiological Protection Principles concerning the Natural Radioactivity of

Building Materials" . Radiation protection 112.

El Aassy, I.E., Afaf, A., Nada, B.N., El Galy, M.M., El Feky, M.G., Abd El., Maksoud, T.M., Talaat, Sh.M., and Ibrahim, E.M. (2012): Behavior and environmental impacts of radionuclides during the hydrometallurgy of calcareous and argillaceous rocks, southwestern Sinai, Egypt.Nuclear Materials Authority, Egypt, Faculty of Women for Arts, Science and Education, Egypt.

El Afandy AH, and El Shaib GB (2020). Geology and distribution of radioelememnts as well as environmental impacts at Abu Marw younger granites, Southeastern Desert, Egypt. Egyptian Journal of Geology, Accepted.

El Afandy AH, El Kammar A.A., Abdel Gawad, A.E., and Rizk, T.N. (2018): Distribution of radionuclides in uraniferous two mica granites and their environmental inpact at El Sela shear zone, Southern Eastern Desert, Egypt., Nuclear Sciences Scientific Journal, V:7, 135-149.

El Galy, A.M. El Mezayn, Said, El Mowafy A.A., and Mohamed M.S. (2008): Distribution and environmental impacts of some Radionuclides in sedimentary rocks at WadiNaseib area, southwest Sinai, Egypt, Journal of Environmental Radioactivity 99 (2008) 1075-1082.

Fares S, Ashour A, El-Ashry M, and Abd El-Rahma M. (2012). Gamma Radiation Hazardsand Risks Associated withWastes from Granite RockCutting and PolishingIndustries in Egypt. ßäåðîàòàðàä³àö³éîâáåçïåêà 1 (53). ÓÄÊ 539.16:553.521.

Friedrich MH; Cuney M, and Cregu G. (1989). Uranium Enrichment Processes in PeraluminousMagmatism. International Atomic Energy Agency (IAEA)-TC-571/2.11-35.

Fritz H, Abd elsalam M, Ali KA, Bingen B, Collins AS, Fowler AR, Ghebreab W, Hauzenberger CA, Johnson PR, Kusky TM, Macey P, Muhongo S, Stern RJ and Viola G, (2013). Orogen styles in the East African Orogen: a reviewof the Neoproterozoic to Cambrian tectonic evolution. J. Afr. Earth Sci. 86,65– 106.

Gradstein FM, Ogg JG, Smith AG, Bleeker W. and Lourens LJ, (2004). A new geologic time scale with special reference to Precambrian and Neogene. Episodes 27, 83-100.

Hamby DM, and Tynybekov AK. (2000). Uranium, thorium and potassium in soils along the shore of lake IssyK-Kyol in the Kyrghyz Republic. Environ. Monit. Assess. 73, 101-108.

Hamidalddin SHQ. (2012). Study of Natural Radionuclides of some igneous rocks inArabian Shield (South of Al-MadinahAlMunawarah), Saudi Arabia, Journal of American Science 2012;8(12), 1524-1529.

Harb S, El-Kamel AH, Abd El-Mageed AI, Abbady A, & Negm H. (2008). Natural radioactivity measurements in soil Journal of Radiation Research and Applied Sciences 7 (2014) 292-304.

Hargrove US, Stern RJ, Kimura JI, Manton WI. and Johnson PR, (2006). How juvenile is the Arabian-Nubian Shield? Evidence from Nd isotopes and pre-Neoproterozoic inherited zircon in the Bir Umq suture zone, Saudi Arabia. Earth Planet. Sci. Lett. Vol. 252, no. 3-4 pp. 308-326.

Hayumbu P, Zaman MB, Lubaba NCH, Munsanje SS. and Nuleya D. (1995). Natural radioactivity in Zambian building materials collected from Lusaka. Journal of Radioanalytical and Nuclear Chemistry, 199, 229-238.

IAEA Vienna 215-246. Rameshbabu PV. (1999). Rare Metal and Rare Earth Pegmatites of Central India.Special Issue on Rare Metal and Rare Rarth Pegmatites of India. Exploration and Resarch,12, 7-52.

ICRP. (1990). Recommendations of the

International Commission on Radiological Protection, vol. 21 No. 1-3, publication 60.

ICRP. (1994). Protection against radon-222 at home and at work. ICRP Publication 65, 23(2). PergamonPress, Oxford.

International Atomic Energy Agency, (IAEA). (1979). Gamma-ray Surveys in uranium xploration. Technical Reports Series No. 186, Vienna,89 p.

International Atomic Energy Agency, (IAEA). (1996). Internal Basic Safety Standards for Protection against Ionizing Radiation and for the Safety of Radiation Sources. Safety Series No.115

International Atomic Energy, Agency (IAEA). (1989). Measurement of radionuclides in food and the environment, a guidebook, Technical Reports Series No. 229, Vienna.

Kohshi C, Takao I. And Hideo S. (2001). Terrestrial gamma radiation in Koshi prefecture, Japan. Journal of Health Science, 47 (4), 362-372.

Krieger R. (1981). Radioactivity of construction materials. BetonwerkFertigteil-Techn.47, 468-473.

Malczewski D; Taper L, and Dorda J. (2004). Assessment of natural and anthropogenic radioactivity levels in rocks and soils in the environs of Swieradow Zdroj in Sudetes, Poland by in situ gamma-ray spectrometry.J. Environ. Radioact.73, 233e245.

Matolin M. (1991). Construction and Use of Spectrometric Calibration Pads Laboratory • -ray spectrometry, NMA, Egypt. A Report to the Government of the Arab Republic of Egypt. Project EGY/4/030-03.IAEA.

Moghazy NM. (2016). Petrography, Gamma radiation measurements and dose rate, Northeastern Um Ara area, South Eastern Desert, Egypt., Nuclear Sciences Scientific Journal, V:5, 91-108.

Mohd Zubair Deepak VermaAmeer Azam, Sukanta Roy (2013). Natural radioactivity and radiological hazard assessment of soil using gamma-ray spectrometry. Radiat. Prot. Dosimetry, 155 (4): 467-473.

Nada A (2003). Evaluation of natural radionuclides at Um-Greifat area, eastern desert of Egypt. Appl RadiatIsot, 58 :275-280.

Nagdya MI (2003). Radioactive disequilibrium in the different rock types in Wadi Wizr, the Eastern Desert of Egypt. Applied Radiation and Isotopes 58(3):385-392 ·

Orgun Y, AltinsoyN, Sahin SY, Gungor Y, Gultekin AH, Karaham G, and Karaak Z, (2007). Natural and anthropogenic radionuclidesin rocks and beach sands from Ezineregion (canakkale), WesternAnatolia, Turkey. Applied Radiation and Isotopes, 739– 747: 65.

Pal DC; Mishra B, and Bernhardt HJ. (2007). Mineralogy and Geochemistry of Pegmatite-Hosted Sn-, Ta-Nb- and Zr-Hf-Bearing Minerals from the Southereastern Part of the Bastar-Malkangiri Pegmatite Belt, Central India. Ore Geology Reviews, 30, 30-55. .

Poty B; Cuney M, and Friedrich M. (1986). Uranium Deposits Spatially Related to Granites in the French Part of the Hercynian Orogeny, Vein Type Uranium Deposits. IAEA-TECDOC-361,

Quindos LS, Fernández PL, Ródenas C, Gómez-Arozamena J. and Arteche J. (2004). Conversion factors for external gamma dose derived from natural radionuclides in soils. Journal of Environmental Radioactivity, 71, 139-145.

Rameshbabu PV. (1999). Rare Metal and Rare Earth Pegmatites of Central India. Special Issue on Rare Metal and Rare Earth Pegmatites of India. Exploration and Resarch,12, 7-52.

Ravisankar R, Vanasundari K, Chandrasekaran A, Rajalakshmi A,

Suganya M, Vijayagopal P. and Meenakshisundaram V. (2012). Measurement of Natural Radioactivity in Building Materials of Namakkal, Tamil Nadu, India Using Gamma-Ray Spectrometry, Applied Radiation and Isotopes, 70, 699-704.

Serena Righi and Luigi Bruzzi. (2006). Natural radioactivity and radon exhalation inbuilding materials used in Italian dwellings. Journal of Environmental Radioactivity 88 (2006) 158-170.

Sroor A, Abd El Halim ES, El-Shershaby A, Walley El Dine N, and Afifi S. (2012). Evaluation of natural radionuclides for mica and quartz in Eastern Desert of Egypt using gamma ray spectrometry. Journal of Nuclear Physics and Atomic Energy, 13(2).

Stern RJ, (2002). Crustal evolution in the east African Orogen: a neodymium isotope prospective. J. Afr. Earth Sci. 34, 109-117.

Tzortzis M, Tsertos H, Christofides S. and Christodoulides G. (2003). Gamma radiation measurements and dose rates in commercially-used natural tiling rocks (granites). Journal of Environmental Radioactivity, 70, 223-235.

UNSCEAR. (1988). Sources, Effects and Risks of Ionizing Radiation, Report to the General Assembly, United Nations, New York.

UNSCEAR. (1993a). Sources and Effects of Ionizing Radiation. United Nations Scientific Committee on the Effects of Atomic Radiation, United Nations, New York.

UNSCEAR. (1993b). Exposure from natural sources of radiation. Forty-second session of United Nations Scientific Committee on the Effect of Atomic Radiation, Vienna 12-28 May.

UNSCEAR. (2000). United Nations Scientific Committee on the effects of Atomic Radiation. Report to the General Assembly, with scientific annexes. Sources and Effects of Ionizing Radiation. United Nations sales publications No. E.00.IX.3 Volume I: Sources) and No. E.00.IX.4 (Volume II: Effects). United Nations, New York, 1220 pp.

Walley El Dine N, Sroor A, Ali Kh, Ibrahim T, El-Shershaby A, and El Taib Z.(2012). Determination of specific activity of natural radioactivity for assessment of hazard radiation from the Egyptian row materials, Journal of Environmental Science, 41(2), 457-467.

الملخص العربي

عنوان البحث: جيولوجية وبتروجرافية واشعاعية والتأثير البيئي لصخور وادي كاب الركب الشمالي-جنوب الصحراء الشرقية-مصر

منى الحرايرى[١]، عادل الافندى[٢]، هدى رجب سعد*[١]
[١] قسم الجيولوجيا – كلية العلوم – جامعة دمياط – دمياط الجديدة - مصر
[٢] هيئة المواد النووية- القطامية- القاهرة- مصر

يهدف هذا البحث الي دراسة الوضع الجيولوجي لمنطقة وادي كاب الركب الشمالي-جنوب الصحراء الشرقية-مصر وتوزيع العناصر المشعة بها وقياس مخاطر الاشعاع الناتجة من أنواع الصخور المختلفة في هذه المنطقة.
تم دراسة الوضع الجيولوجي للمنطقة تحت الدراسة والتي تتكون من الصخور النارية والمتحولة للبروتيروزي المتاخر والتي تشمل البركانيات المتحولة؛ الجابرو المتحول؛ الجرانوديوريت؛ الجابرو الحديث؛ المنزوجرانيت؛ السيانوجرانيت؛ الجرانيت القلوي والسيانيت القلوي. وكذلك العلاقات الحقلية بين هذه النوعيات المختلفة من الصخور.
أوضحت نتائج الدراسة ان جميع أنواع الصخور تحتوي على تركيزات قليلة من اليورانيوم والثوريوم؛ وبحساب جميع المتغيرات التي تقيم الأثر البيئي لهذه الصخور تبين انها جميعا في النطاق الامن على الانسان إذا استخدمت هذه الصخور في البناء او كاحجار زينة.